Dynamic Measurement of Nanoflows: Analysis and Theory of an Optofluidic Flowmeter

Paul N. Patrone,* Gregory Cooksey, and Anthony Kearsley
National Institute of Standards and Technology
(Dated: February 15, 2019)

Scientists must overcome fundamental measurement problems if microfluidic devices are to become reliable and commercially viable. In particular, microfluidic devices require precise control over operating conditions such as flow-rate, v_v, which is difficult to measure continuously and *in situ*. Given the small scales involved, state-of-the-art approaches generally require accurate models to infer v_v on the basis of indirect measurements. However, such methods necessarily introduce *model-form errors* that dominate at the nL/min scale being targeted by the community. To address these problems, we develop a robust and largely assumption-free scaling method that relates the fluorescence efficiency $\mathcal{I}$ of fluorophores to v_v through a dosage parameter ξ, which depends on the flow rate and laser power. Notably, we show that this scaling relationship emerges as a universal feature from a *general* class of partial differential equations (PDEs) describing the experimental setup, which consists of an excitation beam and fluorescence detector. *As a result, our approach avoids uncertainties associated with most modeling assumptions, e.g. the exact system geometry, the flow profile, the physics of fluorescence, etc.* Moreover, the corresponding measurements remain valid down to the scale of 10 nL/min, with some devices potentially capable of reaching 1 nL/min. As an added benefit, the measurement procedure is mathematically simple, requiring a few trivial computations, as opposed to the full solution of a PDE. To support these claims, we discuss and quantify uncertainties associated with our method and present experimental results that confirm its validity.

I. INTRODUCTION

Accurately measuring flow rates is critical to a variety of microfluidic applications such as droplet formation [1], particle sorting [2], flow cytometry [3], and mixing [4]. However, precise measurements down to the μL/min and nL/min scales are difficult to perform in many settings such as "labs-on-a-chip," where continuous, in-situ monitoring is often necessary for device control. In particular, current techniques: (i) involve large and/or expensive microscopes [5], (ii) require precise information about the geometry of the microchannel (which may be expensive to determine in mass-production settings),[5] and/or (iii) lack high-throughput resolution down to the nL/min scales.[6] As such, there are no commercially available and easy-to-use measurement devices that can be deployed in microfluidic settings at ultra-low flow rates.

Conceptually, the need for *robust and inexpensive uncertainty control* is the key problem that all flow rate measurement techniques attempt to address. The current difficulty in achieving this arises from the *belief* that a precise measurement must fully resolve the microfluidic flow channel (i.e. the microchannel). For example, velocimetry-based approaches visualize individual streamlines,[6] whereas more indirect methods (e.g. based on cantilevers) require expensive simulations and detailed knowledge of the underlying system geometry.[5] Both approaches, however, suffer from the fact that device fabrication uncertainties can propagate into the final measurements in a manner that is inversely proportional to the flow rate. Thus, in order to perform accurate measurements on increasingly small systems, the community needs a new paradigm for controlling uncertainty, i.e. one that does not rely on detailed and/or precise models.

To address these problems, we develop and test a method of in-situ, fluorescence-based flow rate measurements for microfluidic devices that obey scaling relationships derived from a general class of first-order partial differential equations (PDE). In particular, we consider devices of the type illustrated in Figs. 1 and 2 in which a laser (or cascade thereof) induces fluorophores to emit photons while also photobleaching some fraction of the molecules. We show that under a variety of physically realizable conditions, the fluorescence efficiency $\mathcal{I}$ has a *one-to-one, injective* relationship with the dosage $\xi = f(p)/v_v$, where $f(p)$ is some function of the laser power and v_v is the volumetric flow rate. By determining $\mathcal{I}(\xi)$ via a single-point calibration, we can use measurements of this quantity to deduce v_v, given the laser power (which we control). Experimental results confirm the validity of this approach down to flow rates of 10 nL/min and suggest that 1 nL/min is attainable.

A key goal of our work is to highlight the idea that scaling-based measurements are a powerful theoretical tool to overcome the experimental limitations associated with microfluidic devices. In particular, our main result amounts to a mathematical proof that a flow rate measurement can be performed *absent any detailed information about the physics of fluorescence or the system geometry.*[7] As such, precise control over and uncertainty quantification (UQ) of these aspects of the device is entirely unnecessary, which reduces the burden associated with both fabrication and data analysis. Stated differ-

* paul.patrone@nist.gov

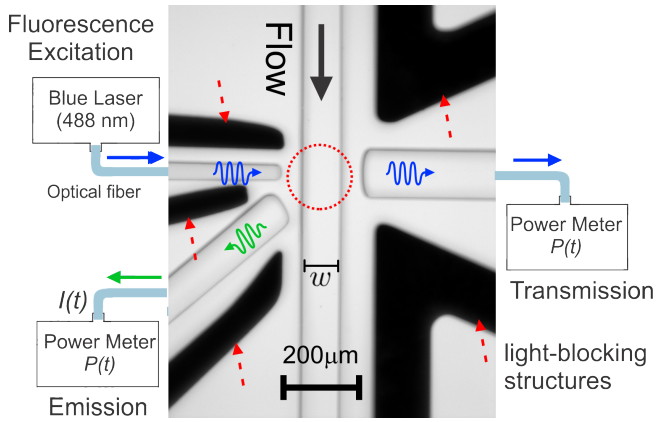

FIG. 1. Close-up view of an individual optofluidic flow-meter. This device is made of PDMS and contains integrated waveguides filled with optical adhesive (Norland 88). A narrow waveguide delivers excitation light to fluorescein in a flow channel while a wider waveguide collects emission light and couples to a power meter (Newport 2936-R) through an emission filter. Flow channel cross section is 100 μm $\times$ 80 μm. See Sec. VII for details on fabrication. See Fig. 2 for a schematic of multiple devices in serial. See Fig. 3 for an example of a flow-meter in operation.

ently, our scaling method facilitates accuracy by eliminating errors associated with using the wrong model to analyze data,[8] since our result applies uniformly to a broad class thereof. Thus, virtually all of the measurement uncertainty is shifted to the time-series data arising from the fluorescence intensity signal, which can be analyzed using a variety of well-established tools.

As regards those uncertainties that are unavoidable, we discuss their origins and propagation into final measurements. Of note, our approach requires a calibration in which the fluorescence efficiency $\mathcal{I}$ is measured at a known flow rate by varying the laser power. This reference flow rate is assumed to be the lower limit of some other well-established device, and importantly, is subject to its own uncertainty. By means of an uncertainty propagation argument, however, we arrive at the interesting result that our scaling method only inherits the relative (but not absolute) uncertainties associated with the reference measurement. *In other words, our scaling method can (in principle) attain the same relative accuracy as a good reference measurement, but at much lower flow rates.*

While the approach we propose is useful for describing a wide range of measurement devices, it does have certain limitations. In particular, the analysis requires that the device operate in either a advection-dominated or Taylor-Aris-diffusion regime. Physically, these restrictions amount to the requirement that the axial fluid motion be dominated by a single timescale, namely that of the volumetric flow rate. Nonetheless, we present perturbation arguments and experimental results showing that these regimes are easily accessible to typical microfluidic devices at flow rates of interest. Indeed, we

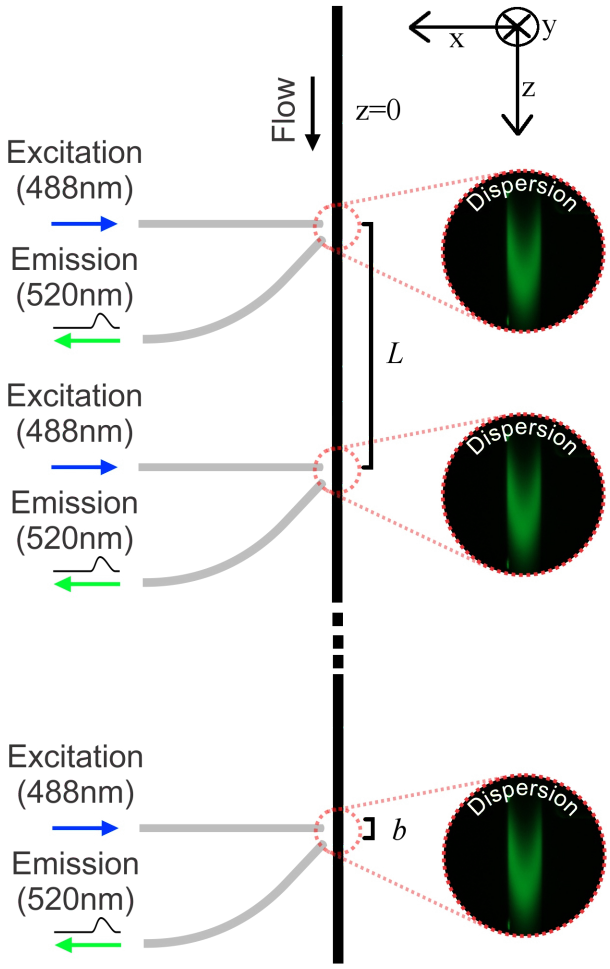

FIG. 2. Schematic of the microfluidic device we consider. Fluid containing a fluorescent marker (e.g. fluorescein) flows down the channel in the z-direction towards a 488 nm excitation laser. Once in the laser-beam, fluorescein molecules emit fluorescent 520 nm light, which is collected by an appropriate detector. Several devices can be positioned in serial to measure flow rates at different positions along the channel, although only a single device is actually required to measure the flow rate. The characteristic lengh of the laser profile in the z-direction is denoted b, whereas the separation between lasers is L. See Fig. 1 for a close-up view of an individual optofluidic flowmeter.

anticipate that the Taylor-Aris regime could allow for measurements of flow rates *below* the nL/min scale, the latter being widely considered as an important goalpost in microfluidics.

The rest of this manuscript is organized as follows. Section II discusses a linear version of our model and highlights key assumptions. Section III derives the scaling relationship that forms the basis for our measurement technique. Section IV discusses a broad generalization of the linear analysis that extends its validity the situation in which the physics of photobleaching and fluorescence is unknown and highly non-linear. Section V discusses sources of uncertainty and presents a basic uncertainty

propagation argument associated with the reference measurement. Section VI discusses heuristic device optimization considerations that facilitate measurements. Section VII shows experimental results that confirm our theory. Section VIII provides a broader discussion of our work and reviews main conclusions.

A. Notation and terminology

We use the following notation and terminology throughout:

- We refer to the z-axis as the axial direction, while we refer to the x-y plane as the radial direction.
- $\mathbf{r} = (x, y, z)$ denotes a coordinate in $\mathbb{R}^3$.
- c denotes the concentration of unbleached fluorophores.
- c_0 denotes the total concentration of fluorophores, bleached and unbleached. Therefore, $c_0 - c$ is the concentration of bleached fluorophores.
- D denotes the diffusion coefficient of fluorophores.
- p is a dimensionless parameter corresponding to the laser power. In particular, we restrict $0 \leq p \leq 1$, where $p = 0$ corresponds to the laser being off, and $p = 1$ corresponds to the laser being at full power. When considering a system with more than one laser, we denote the corresponding laser powers as p_k.
- $I_k(t)$ denotes the (time-dependent) fluorescence-intensity signal collected at the kth laser.
- $\mathcal{I}_k = I_k(t \to \infty)/p_k$ is the steady-state fluorescence efficiency, i.e. the fluorescence per-unit-laser-power associated with the intensity collected at the kth laser.
- v_v denotes the volumetric flow rate.
- $\xi = f(p)/v_v$ is a scaling parameter that we refer to as the dosage, where $f(p)$ is a function of the laser power that has units of inverse time.[9] We generally assume that $f(p)$ is a monotone increasing function (see below) in p. Thus increasing the laser power or decreasing the flow rate increases the dosage. For systems with more than one laser, we denote the corresponding dosages as $\xi_k = f(p_k)/v_v$.
- A monotone increasing (decreasing) function $f(x)$ is one for which $f(x_1) \geq f(x_2)$ $[f(x_1) \leq f(x_2)]$ if $x_1 > x_2$.
- A strongly monotone increasing (decreasing) function is one for which $f(x_1) > f(x_2)$ $[f(x_1) < f(x_2)]$ if $x_1 > x_2$.
- A bijection $f(x)$ on a domain U is a function such that every f in the range $f(U)$ corresponds to exactly one element x in U. A strongly monotone function is a bijection.[10]

II. ASSUMPTIONS AND MODEL EQUATIONS

In order to make the analysis that follows more accessible, we begin with a simplified model of the device that assumes photobleaching and fluorescence depend linearly on the concentration c of the fluorescent molecule (fluorescein in our experiments). While this assumption is not strictly necessary, it has the benefit of allowing us to write formally exact expressions for the measurement signal $\mathcal{I}$. In Sec. IV, we distill this model to its essence by showing that the full weight of our analysis applies even when photo-bleaching and fluorescence are highly non-linear processes, provided they are monotone in c.

A. System geometry and flow-profile

Consider a flow channel (or duct) oriented in such a way that the fluid travels in the z-direction. The channel cross-section lies in the perpendicular $x-y$ plane and has a characteristic width w. Let N laser beams be placed along the z-direction, with adjacent beams separated by a "center-to-center" distance L. Assume that L is larger than the beam-length b (in the z-direction), so that no two beams overlap; see Figs. 1 and 2. We denote $\mathcal{L}$ as the characteristic length of the device, where $\mathcal{L} = b$ is the length of a single laser if $N = 1$, and $\mathcal{L} = NL$ if $N > 1$. We also assume that the flow is laminar and Poiseuille, and that the channel dimensions are constant over the distance $\mathcal{L}$.

As the flow is Poiseuille, we may assume that its velocity profile can be expressed as $v_v u(x, y)$, where $u(x, y)$ is a fixed function that describes the position-dependence of the flow. This factorization implies that $u(x, y)$ satisfies

$$1 = \int \mathrm{d}x\, \mathrm{d}y\, u(x, y), \tag{1}$$

an observation that is useful in a certain limiting case.

Before continuing, we note that the assumption of Poiseuille flow requires the Reynolds number R to be sufficiently small, i.e. $R \lesssim 10^3$. For the system under consideration,

$$R = \frac{v_c w}{\mu_k} = \frac{v_v}{w \mu_k}, \tag{2}$$

where $v_c = v_v/w^2$ is the characteristic linear velocity of the flow and μ_k is the kinematic viscosity of the fluid. Thus, a proportional decrease in both v_v and w keeps R the same. In Sec. VI, we consider these quantities in the context of the experimental setup.

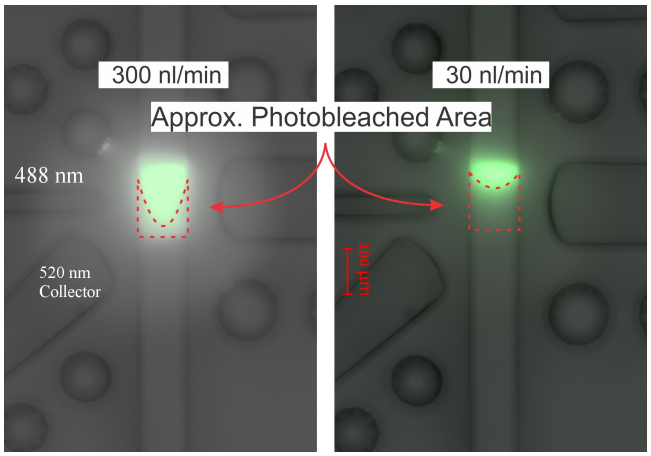

FIG. 3. Microscope view of a typical flow-meter in operation at different flow rates. The laser is labeled 488 nm, while the fluorescence collector is labeled 520 nm. Note that decreasing the flow-rate increases the amount of bleaching.

B. Linear model equations

With the geometry described above, we can express the system evolution via the equations

$$\partial_t c = D\nabla^2 c - v_v u(x,y)\partial_z c - \sum_k p_k \phi_k(\mathbf{r}) c \tag{3a}$$

$$\partial_x c = \partial_y c = 0 \qquad \mathbf{r} \in \partial U \tag{3b}$$

$$c \to c_0 \qquad z \to \pm\infty \tag{3c}$$

$$c(\mathbf{r}, t=0) = c_0 \tag{3d}$$

$$I_k(t) = \int \mathrm{d}\mathbf{r}\; p_k \phi_k(\mathbf{r}) c(\mathbf{r}, t). \tag{3e}$$

Interpretation of Eq. (3a) is straightforward: unbleached particles diffuse at a constant rate D, advect at the velocity $v_v u(x,y)$, and are destroyed at a rate of $f(p_k) = p_k\phi_k(\mathbf{r})$ by the kth laser, where $\phi_k(\mathbf{r}) \geq 0$ characterizes the relative intensity of laser-light in the channel. Equation (3b) states that no fluorophores leave the channel through its boundary ∂U, while Eq. (3c) forces the concentration of unbleached molecules to tend towards its initial value far from the experimental lasers along the flow direction. The measured intensity of fluorescent light at the kth laser, given by Eq. (3e), is simply the "sum over probabilities" (i.e. an integral) that unbleached particles fluoresce. See also Fig. 3.

We note in passing that the term $\phi_k(\mathbf{r})$ plays multiple roles in this model. In addition to characterizing the intensity of light, it also accounts for: (i) the probability of a molecule being photobleached [Eq. (3a)]; (ii) the probability of fluorescing [Eq. (3e)]; and (iii) geometrical factors associated with the fraction of fluorescent photons that actually arrive at the detector [Eq. (3e)]. While we have no reason to believe that the same ϕ_k describes all of these effects, it is reasonable (in the context of a linear model) to assume that they are proportional to ϕ_k. As such, we may informally view I_k as the fluorescence intensity scaled by the bleaching rate, or vice versa. *However, such considerations play no role in our final measurement procedure, an observation that amounts to one of our key conclusions.* These points in particular will become more apparent in Sec. IV when we generalize to arbitrary bleaching and fluorescence models.

C. First-order models

For the purposes of measurement, Eqs. (3a) and (3e) are difficult to work with by virtue of the diffusion term. That is, the defining characteristic of diffusion is its ability to smear out signals, which often manifests as noise. At a minimum, this motivates us to seek operating conditions in which diffusion is (effectively) negligible. We consider two distinct regimes: (i) $D \to 0$, i.e. slow diffusion; and (ii) the limit of fast radial diffusion.

1. *Limiting case of slow diffusion*

Consider a rescaling of Eq. (3a) as follows. Denote $x = w\chi$, $y = w\gamma$, and $z = \mathcal{L}\zeta$, and let $A = \mathcal{L}/w$ be the axial aspect ratio of the duct. Rewriting Eq. (3a) in these variables yields

$$c_t = \frac{D}{\mathcal{L}^2}\left[A^2(c_{\chi,\chi} + \partial_{\gamma,\gamma}) + c_{\zeta,\zeta}\right] - \frac{v_v u}{\mathcal{L}} c_\zeta - Bc, \tag{4}$$

where $B = \sum_k p_k \phi_k(\mathbf{r})$ is the bleaching term. Next, define $u = \mathfrak{u}/w^2$, and recall that v_v/w^2 is the characteristic linear velocity of the flow profile. Dividing by this last quantity and letting $\tilde{t}$ and $\tilde{B}$ be the corresponding rescaled time and bleaching function (whose precise forms are not important here), we find

$$c_{\tilde{t}} = P^{-1} c_{\zeta\zeta} + P_{\text{eff}}^{-1}(c_{\chi\chi} + c_{\gamma\gamma}) - \mathfrak{u} c_\zeta + \tilde{B}c, \tag{5}$$

where

$$P = \frac{v_v \mathcal{L}}{w^2 D} \tag{6a}$$

$$P_{\text{eff}} = \frac{P}{A^2} = \frac{v_v}{\mathcal{L} D} \tag{6b}$$

are the Peclet and effective Peclet numbers, respectively. Physically, P characterizes the relative rates of axial transport versus axial diffusion; P_{eff} characterizes the relative rates of axial transport versus radial diffusion.

A few comments are in order. First, when both P and P_{eff} are large, singular perturbation arguments tell us that omitting the diffusion terms results in errors that are $\mathcal{O}(P^{-1} + P_{\text{eff}}^{-1})$. Therefore, we (approximately) minimize the error by minimizing this sum as a function of the duct geometry and $\mathcal{L}$. Assuming, a fixed cross-sectional area w^2, diffusion constant D, and volumetric flow rate, we find that $\mathcal{L} = w$, or equivalently $A = 1$, minimizes the sum $P^{-1} + P_{\text{eff}}^{-1}$. This implies that

$P = P_{\text{eff}} = v_v/\mathcal{L}D = v_v/wD$, i.e. the two Peclet numbers are equal. Physically, this observation is interesting because at first glance, it is counter-intuitive. Naively one expects that we should make $\mathcal{L}$ as small as possible because doing so reduces the time for diffusion to act, thereby reducing noise. However, considering that we can also express P as the ratio of characteristic diffusion and advection times (i.e. $P = \tau_D/\tau_v$), one see that at short distances, axial diffusion acts faster than advection, so that we in fact *increase* noise by making $\mathcal{L}$ too small.

Second, when considering an optimal geometry (i.e. $A = 1$), we conclude that for a fixed Peclet number, decreasing the volumetric flow rate requires a proportional decrease in w. In other words, a system for which $v_v = 1$ μL/min and $w = 100$ microns has the same Peclet number as a system for which $v_v = 10$ nL/min and $w = 1$ micron. As we will see, this imposes practical lower bounds on the volumetric flow rates that we can realistically hope to model in this regime.

Assuming now that the Peclet numbers are sufficiently large, we drop the second order derivatives to arrive at the reduced model

$$c_\tau = -u(x,y)c_z - \sum_k \xi_k \phi_k(\mathbf{r})c, \tag{7}$$

where $\tau = v_v t$. Since Eq. (7) contains no derivatives in either x or y, these quantities have effectively become free parameters of the model, as opposed to independent variables. As such, we may henceforth assume that their values are fixed.

2. *Limiting case of fast radial diffusion*

The Peclet numbers given in Eqs. (6a) and (6b) have a reciprocal dependence on the length-scale $\mathcal{L}$. As such, it is possible to take a limit in which $P \propto \mathcal{L}v_v/w^2 \to \infty$ and $P_{\text{eff}} \propto v_v/\mathcal{L} \to 0$, which, importantly, encompasses the case $v_v \to 0$. In this situation, Eq. (3a) reverts to the singular limit

$$c_{\tilde{t}} = P_{\text{eff}}^{-1}(c_{\chi\chi} + c_{\gamma\gamma}) - \mathfrak{u}c_\zeta + \tilde{B}c, \tag{8}$$

when expressed in terms of the rescaled variables of the previous section. In this limit, diffusion only takes place in the radial direction, and importantly, does so at a rate that is fast relative to advection. With this physical picture in mind, we now show that Eq. (8) amounts to a special case of Eq. (7).

Assume that $P_{\text{eff}} \ll 1$ and express c as a power series of the form

$$c = c^{(0)} + P_{\text{eff}}c^{(1)} + P_{\text{eff}}^2 c^{(2)} ... = \sum_j c^{(j)} P_{\text{eff}}^j, \tag{9}$$

where $c^{(j)}$ are perturbations to the concentration field that we must determine systematically. Inserting this expansion into Eq. (8) and applying the principle of dominant balance,[11] we find to $\mathcal{O}(P_{\text{eff}}^{-1})$ that

$$c^{(0)}_{\chi,\chi} + c^{(0)}_{\gamma,\gamma} = 0. \tag{10}$$

As ζ does not appear in this equation, we find (by virtue of the no-flux boundary conditions) that $c^{(0)} = c^{(0)}(\zeta)$ is a function only of ζ. However, this is not sufficient to actually determine the leading order concentration. To do this, we consider the $\mathcal{O}(1)$ term of Eq. (8),

$$c^{(0)}_{\tilde{t}} = (c^{(1)}_{\chi,\chi} + c^{(1)}_{\gamma\gamma}) - \mathfrak{u}c^{(0)}_\zeta + \tilde{B}c^{(0)}, \tag{11}$$

which couples $c^{(0)}$ and $c^{(1)}$. Next, integrate Eq. (11) over χ and γ. Applying the no-flux boundary conditions eliminates the first-order correction to c, yielding the PDE

$$c^{(0)}_\tau = -a^{-1}c^{(0)}_z - \sum_k \xi_k \bar{\phi}_k(\mathbf{r})c^{(0)} \tag{12}$$

where $a = \int \mathrm{d}x\,\mathrm{d}y$ is the cross-sectional area and $\bar{\phi}_k(z) = a^{-1}\int \mathrm{d}x\,\mathrm{d}y\,\phi_k(x,y,z)$ is the normalized radial average of the intensity profile. Note that in arriving at Eq. (12) we have also invoked Eq. (1).

Several comments are in order. For one, Eq. (12) is of the same form as Eq. (7), except that the velocity profile is now a constant and the laser intensity is a function of z alone. As such, any analysis applicable to the more general Eq. (7) also applies to Eq. (12). Physically, we can understand this singular limit as follows. As $P_{\text{eff}} \to 0$ and $P \to \infty$, radial diffusion is so fast (compared to advection) that any given fluorophore explores the entire radial dimension of the flow profile before advancing significantly in the flow direction. In other words, it "sees" the average flow velocity, which is a constant. By Eq. (9), we anticipate that this approximation has errors on the order of P_{eff}, which can be controlled through device construction.

As an interesting aside, we note that under certain experimentally attainable conditions, the flow-profile u can be independent of the radial coordinates.[12] If the laser profile $\phi(\mathbf{r}) = \phi(z)$ is likewise only a function of the axial variable, it is possible to integrate Eq. (8) directly in x and y without the need to perform a perturbation expansion in the spirit of Eq. (9). In retrospect, this is perhaps not surprising, since a constant velocity profile and laser intensity effectively reduce the physics of light-matter interactions to a one-dimensional problem. Nonetheless, it is reassuring that the analysis holds in this degenerate case.

III. SCALING RELATIONSHIPS AS THE BASIS FOR MEASUREMENT

Stated simply, the goal of building and modeling the measurement device is to be able to associate a given flow rate v_v with one or more measured intensity curves $I_k(t)$.

Because any given signal $I_k(t)$ is generated as a time-series of data, however, we face the prospect of mapping a function to a scalar, which may not be straightforward if $I_k(t)$ is noisy. This motivates us to instead study the relationship between v_v and $I_{k,s} = I_k(t \to \infty)$; that is, we treat the steady-state (and thus scalar) intensity as the desired measurement, ignoring any transient effects associated with, e.g. turning on a laser or injecting fluorophores.

We therefore set $c_\tau = 0$ in Eq. (7), which yields the expression

$$c_z = -\frac{1}{u(x,y)} \sum_k \xi_k \phi_k(\mathbf{r}) c. \tag{13}$$

Recalling that $u(x,y)$ and $\phi_k(\mathbf{r})$ are fixed and independent of the volumetric flow rate, we see that the governing equation depends only on the dosage rate $\xi_k = p_k/v_v$. In other words, simultaneously decreasing the power and flow rate by the same factor leaves the concentration of unbleached fluorophores unchanged.

To see this more explicitly, we construct a formally exact solution to the steady-state equation. In particular, Eq. (13) has been reduced to an ordinary differential equation that can be integrated exactly. One finds

$$c_s(\mathbf{r}) = c_0 \exp\left[-\sum_k \xi_k \Phi_k(\mathbf{r})\right], \tag{14}$$

where

$$\Phi_k(x,y,z) = \frac{1}{u(x,y)} \int_0^z \mathrm{d}z'\, \phi_k(x,y,z') \tag{15}$$

and $z = 0$ is some position upstream of the first laser (cf. Fig. 2). Physically, we interpret $\xi_k \Phi_k$ as the *total* dosage of radiation from the kth laser received by a fluorophore molecule as it travels down the channel. Note that $\Phi_k(x,y,z \le 0) = 0$, while $\Phi_k(x,y,z \ge z_{\max}) = \Phi_{k,s}(x,y)$ is independent of z for some $z_{\max}$, since the laser beams only illuminate a narrow strip. In other words, $\xi_k \Phi_{k,s}(x,y)$ is the total dosage of radiation delivered to a molecule having completely passed the kth laser. *It is important to note in particular that* $\Phi_k \ge 0$ *and that* $\Phi_{k,s} > 0$.

Given Eq. (14), the steady-state fluorescence intensity collected at the kth laser is given by

$$\mathcal{I}_k := \frac{I_{k,s}}{p_k} = \int_{U_k} \mathrm{d}\mathbf{r}\, c_0\, \phi_k(\mathbf{r}) \exp\left[-\sum_{j=1}^{k} \xi_j \Phi_j(\mathbf{r})\right], \tag{16}$$

where U_k is the domain illuminated by the laser.[13] Note that for $k > 1$, the sum appearing in the integral reduces to

$$\sum_{j=1}^{k} \xi_j \Phi_j(\mathbf{r}) = \xi_k \Phi_k(\mathbf{r}) + \sum_{j=1}^{k-1} \xi_j \Phi_{j,s}(x,y) \tag{17}$$

by virtue of the fact that the fluorescein molecules have completely passed the first $k-1$ lasers and now reside entirely in the kth.

Recall that we interpret the scaled intensity $\mathcal{I}_k$ as the fluorescence per unit of laser-power. *Critically, it is straightforward to show that* $\mathcal{I}_k$ *is a strictly monotone decreasing function of the scaling parameters* $\xi_k = p_k/\alpha$, *given that the* $\Phi_k(\mathbf{r})$ *are positive in the domains* U_k. To understand this physically, note that increasing the dosage bleaches more particles, so that fewer are available to fluoresce; thus, the fluorescence efficiency decreases per unit of input power. Consider also that the intensity $\mathcal{I}_k$ only depends on the power of the first k lasers. Mathematically, we can express these observations by noting that the scaled intensity $\mathcal{I}_k$ takes the arguments $(\xi_1, \xi_2, ..., \xi_k)$. If we further require that the laser powers are coupled (which can be achieved experimentally via wave-guide splitters), then we find that $p_k = p f_k$, where p is the power shared by all lasers and f_k is the fixed fraction received by the kth. Under these conditions, $\mathcal{I}_k$ reduces to a simpler function

$$\mathcal{I}_k(\xi_1, \xi_2, ..., \xi_k) \to \mathcal{I}_k(\xi), \tag{18}$$

which is a function of only one similarity variable.

Practically speaking, Eq. (18) can be used as the basis for a measurement device as follows. First, assume that we can measure the volumetric flow rate v_v using some second device, and refer to this rate as the reference rate v_r. We desire v_r to be at the lower limit (for example) of the measurement capability of this latter device, since the goal is to extend measurement capabilities to lower flow rates using $\mathcal{I}$. Knowing v_r, we then vary the power p, which amounts to changing $\xi = p/v_r$. While doing this, we measure the intensity I_k, which thereby maps out the function $\mathcal{I}_k(\xi)$. See Fig. 4.

To actually measure an unknown v_v, we reverse the above procedure, fixing $p = p_m$ and varying the flow rate. Given the intensity measurement $\mathcal{I}_m$ associated with this flow rate, we use the previously-determined mapping $\xi \mapsto \mathcal{I}_k$ to identify the corresponding $\xi_m = p_m/v_v$, which thereby determines

$$v_v = \frac{p_m}{\xi_m}. \tag{19}$$

where p_m is fixed and known. Note that by definition of ξ, we can rewrite Eq. (19) as

$$v_v = \frac{p_m}{p_c} v_r \tag{20}$$

where p_c is the power for which $\xi_m = p_c/v_r$ is satisfied. From Eq. (20), we observe that measuring flow rates less than v_r entails decreasing the measurement power $p_m < p_c$, since the ratio $\alpha = p_m/p_c < 1$. In other words, we only define ξ on the domain $[0, 1/v_r]$, so that decreasing v_v relative to v_r requires a proportional decrease or more in p to stay in this domain. See Fig. 4.

We emphasize that the procedure leading to Eq. (19) takes place without any explicit knowledge of: (i) the

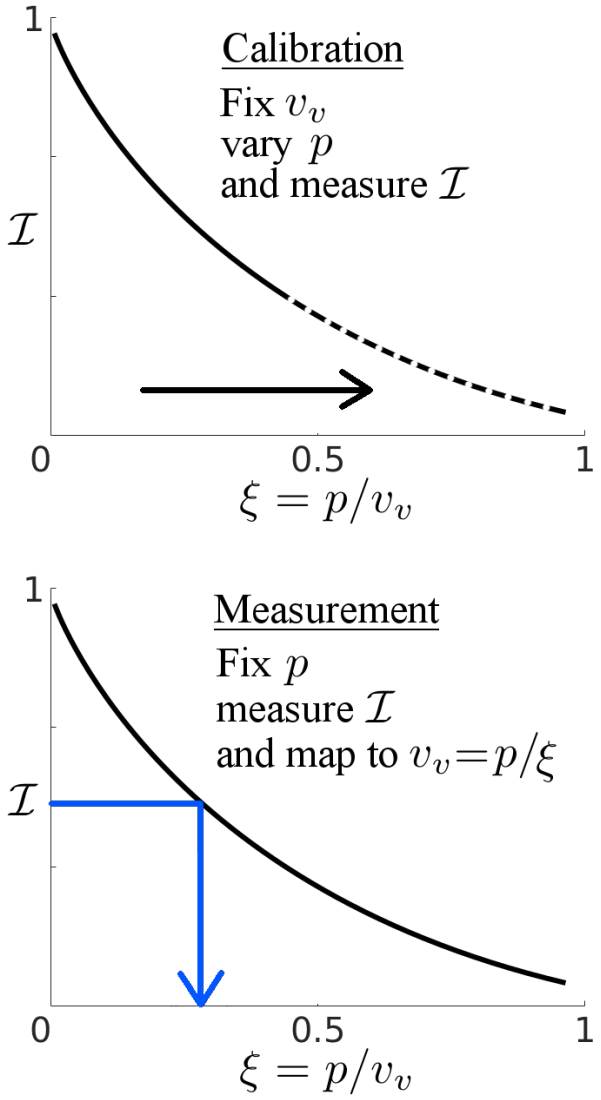

FIG. 4. Illustration of device calibration and measurement. *Top:* To calibrate the device, fix the flow rate at a known value and vary the power while measuring $\mathcal{I}$. This generates the curve $\mathcal{I}(\xi)$. *Bottom:* To determine an unknown flow rate, fix the power at a known value and measure the intensity $\mathcal{I}$. Because $\mathcal{I}(\xi)$ is a bijection, there is a unique ξ corresponding to the measured $\mathcal{I}$, from which we compute $v_v = p/\xi$.

system geometry; (ii) the laser profile; or (iii) the rates of fluorescence. All that has been assumed are order-of-magnitude estimates of the system size, as well as linearity of the bleaching and fluorescence processes. As such, the analysis is essentially immune to uncertainties arising from these sources and can be performed without the need to precisely control the device fabrication. In essence, we have actually avoided these problems by directly *measuring* the steady-state of Eq. (3e), which is a projection of the full solution of Eq. (3a) onto a scalar.

IV. GENERALIZATION TO NONLINEAR MODEL

In general, we have no reason to believe that bleaching is linear in the laser power. In fact, experimental evidence suggests that for widely available fluorophores, such processes often occur through reaction pathways that involve multiple photons, and hence have a dependence on p and/or ξ that is non-linear.[14–18] Fortunately, the analysis discussed in the previous section is easily generalized to account for such cases.

Returning to Eqs. (7) and (3e), we replace the linear interaction terms with a model of the form

$$c_\tau = -u(x,y)c_z - g(\xi)B(c,\mathbf{r}) \tag{21}$$

$$\mathcal{I} = \int \mathrm{d}\mathbf{r}\; F(c,\mathbf{r}) \tag{22}$$

where $\xi = f(p)/v_v$ is a possibly nonlinear function of p, and $B(c,\mathbf{r})$ and $F(c,\mathbf{r})$ are functions of $c(\mathbf{r})$ with compact support in some domain of $\mathbf{r}$ that we call the laser. We assume that $g(\xi)$, $B(c,\mathbf{r})$, and $F(c,\mathbf{r})$ are independent of time, since these functions characterize generic properties of light-matter interactions. We further assume that $B(c,\mathbf{r})$: (i) is non-negative and bounded; and (ii) vanishes (i.e. $B \to 0$) as $c \to 0$.[19] We likewise assume that $f(p) \geq 0$, $g(\xi) > 0$ and $F(c,\mathbf{r}) \geq 0$ are strongly monotone functions in p, ξ and c, respectively.

While these conditions may seem abstract, they have straightforward interpretations. Physically, monotonicity entails that higher concentrations and laser powers lead to more bleaching and fluorescence. Moreover, the compact support assumption amounts to the requirement that bleaching and fluorescence only happen within some finite region that we call the laser. These assumptions are in fact *so general* that for most systems, there are likely few (if any) grounds upon which to challenge them. It is worth noting, however, that we have assumed that the fluorescence is linear in laser power by virtue of the scaling in $\mathcal{I}$. This is likely reasonable in that fluorescence is generally understood to occur through spontaneous emission following absorption of a *single* photon.[20]

Given these assumptions, we seek to show that $\mathcal{I}$ is a bijection of ξ, since this is all that is needed to define the measurement signal. In particular, first note that Eq. (21) admits a steady-state, solution. Setting $c_t = 0$ in Eq. (21) yields a nonlinear ordinary differential equation

$$u(x,y)c_z = -g(\xi)B(c), \tag{23}$$

which has a unique and continuous solution.[21] Formally, this solution can be expressed as

$$c(x,y,z) = \frac{-g(\xi)}{u(x,y)} \int_0^z \mathrm{d}z' B(c(x,y,z'),\mathbf{r}). \tag{24}$$

Using the monotonicity of B and g (along with continuity of c), it is then possible to show that c is in fact a strongly monotone decreasing function of the dosage; see

Appendix A. This coupled with the monotonicity of F proves that $I(\xi)$ is a bijection, as required.

From a practical standpoint, it is important to note that the measurement procedure is slightly modified in the non-linear case if $f(p) \neq p$. Specifically, we find that

$$v_v = \alpha v_r = \frac{f(p_m)}{f(p_c)} v_r \tag{25}$$

so that knowledge of f is required to compute the flow rate. This situation may arise, for example, if the laser intensity is strong enough for bleaching to occur through multi-photon pathways,[14, 15, 20] and for many fluorophores the precise form of $f(p)$ remains unknown. As we demonstrate in Sec. VII, however, it is possible to determine these functions by means of multiple datasets obtained from several known flow rates operating near the lower limit of the reference device. Alternatively, new experiments can be designed to elicit $f(p)$, since this quantity is flow rate independent; see Sec. VIII C.

V. UNCERTAINTY QUANTIFICATION

In Secs. II C and II C 2, we discussed uncertainties arising from the singular perturbation approximations in which the various Peclet numbers take limiting values. Sections III and IV also demonstrated that characteristic (but not exact!) length scales are sufficient to establish the existence of the measurement signal. If we temporarily assume that such uncertainties are negligible, the only remaining potential sources are: (i) the reference flow rate v_r; the laser power p and function $f(p)$; and intensity measurements I. Of these, uncertainty in the reference flow rate is the most interesting, since we cannot necessarily control it through better experimental procedures. We therefore explore its impact on our measurement.

For convenience, we restrict our attention to a single laser and drop the subscript k. Assuming that p, $f(p)$, and I have known, exact values, we recall that an unknown flow rate is determined via the expression

$$v_v = \alpha v_r. \tag{26}$$

Generally speaking, the goal of this calibration exercise is to measure v_r at the upper limit of our device using a tool for which v_r is a lower limit. Thus, we assume that $\alpha < 1$. Letting $v_r = \bar{v}_r + \epsilon_r$, where $\bar{v}_r$ is the true flow-velocity and ϵ_r is the uncertainty associated with the reference measurement, we see that

$$v_v = \bar{v}_v + \alpha\epsilon_r, \tag{27}$$

where $\bar{v}_v = \alpha\bar{v}_r < \bar{v}_r$. *Remarkably, this implies that the relative error of our flow-meter is the same as that of the calibration device;* i.e. $\alpha\epsilon/\bar{v}_v = \epsilon/\bar{v}_r$. Thus, in the idealized case, the scaling method reduces the absolute magnitude of the measurement error while keeping the relative error constant.

In practice, Eq. (27) may underestimate the uncertainty in v_v by virtue of the fact that neither $\mathcal{I}$ nor $\alpha = f(p_m)/f(p_c)$ can be determined exactly. This issue in particular is likely to be important for traceable and commercial applications of the procedure we discuss. However, the corresponding UQ is a challenging task in and of itself and depends on factors external to the device fabrication, e.g. the quality of a given power-sensor. As such, consideration of these issues is beyond our current scope and will be pursued in a subsequent manuscript. When discussing experimental results, however, we indirectly estimate the effects of such uncertainties and their propagation into final measurements; see Sec. VII.

VI. ESTIMATES OF REYNOLDS AND PECLET NUMBERS FOR PRACTICAL DEVICES

Validity of the scaling method relies on being in a advection-dominated or Taylor-Aris regime. In this section, we explore the feasibility of constructing devices that meet these requirements.

Recall that

$$R = \frac{v_v}{w\mu_k}, \tag{28a}$$

$$P = A\frac{v_v}{wD} \tag{28b}$$

$$P_{\text{eff}} = \frac{v_v}{\mathcal{L}D} \tag{28c}$$

where $A = \mathcal{L}/w$ is the aspect ratio. At 293 K, the kinematic viscosity for water is roughly $\mu_k = 1 \times 10^{-6}$ m^2/s. The diffusion coefficient for a fluorophore such as fluorescein is roughly $D = 4\times10^{-10}$ m^2/s. If we take $v_v = V \times 1$ microliter per second (i.e. 1×10^{-9} m^3/s), $w = W \times 1$ micron (i.e. 1×10^{-6} m), and $\mathcal{L} = \mathfrak{L} \times 1$ micron, we find that

$$R = \frac{V}{W} \times 10^3, \tag{29a}$$

$$P = A\frac{V}{4W} \times 10^7 \tag{29b}$$

$$P_{\text{eff}} = \frac{V}{4\mathfrak{L}} \times 10^7. \tag{29c}$$

For an aspect ratio $A = 1$, the last two reduce to $P = P_{\text{eff}} = (V/4W) \times 10^7$. Thus, for a flow of one microliter per second ($V = 1$) and a channel width of 100 microns ($W = 100$), we find $R = 10$ and $P = 2.5 \times 10^4$, which is well within the regime of interest. Dividing by 60 corresponds to a flow rate of 1 microliter per minute, for which $P \approx 400$. In such circumstances, we anticipate that errors associated with neglecting diffusion should be on the order of $P^{-1} \lesssim 1\%$. A device with such dimensions could even conceivably operated down to 100 nL/min, although errors may grow upwards of a few percent.

Reducing the volumetric flow rate to 1 nanoliter per second (i.e. $V = 0.001$) and the system dimensions to

$W = 1$ micron yields $R = 1$ and $P = 2.5 \times 10^3$. In reality, it is probably difficult to achieve a beam width of 1 micron, so that such a device would likely have only a single laser. In this setup, 1 nL/min may in fact be possible, although $P \approx 40$ implies that uncertainties would not necessarily be negligible. However, it is likely that reducing the characteristic device width down to 200 nm or possibly even 400 nm would be sufficient to yield acceptable uncertainties.

In order to reach even lower flow rates, two options exist. First, it is possible to use a slower-diffusion fluorescein-based compound,[22–24] which can reduce the Peclet numbers (and thereby also the uncertainties) by up to a factor of 60. In this situation, a advection-dominated device with $W = 100$ would have diffusion errors on the order of 1/24000 at 1 μL/min. Pushing down to 10 nL/min should therefore only introduce errors on the order of roughly 1/250. Decreasing the channel width to $W = 10$ would correspondingly allow one to reach 1 nL/min with the same errors from diffusion.

An alternative is to use a Taylor-Aris flow-meter with regular fluorescein. Letting $V = 10^{-4}$ (corresponding to 6 nL/min), $W = 1$, $\mathfrak{L} = A = 10000$ (corresponding to a beam-length of 1 cm) gives $R < 1$, $P > 10^5$, and $P_{\text{eff}} \lesssim 1/40$. In this scenario, the Taylor-Aris device would have diffusion-errors comparable to a advection-dominated device. Further reducing the flow rate would, however, *improve* the accuracy of the Taylor-Aris device while degrading that of its advection-dominated counterpart. Thus, there may be an overlap regime where both devices can be used, which has implications for calibration; see Sec. VIII B.

VII. EXPERIMENTAL VALIDATION OF THE THEORY

A. Experimental Methods

1. Photolithography and device fabrication

To test the validity of the scaling approach, we constructed optofluidic flowmeters as illustrated, for example, in Fig. 1. Figures 3 and 5 show related devices in operation. These optofluidic flowmeters were fabricated from master templates by micromolding of poly(dimethylsiloxane) (PDMS) (Sylgard 184, Dow Corning) using soft lithography methods.[25, 26] Photolithography was conducted at the Center of Nanoscale Technology (CNST) at the National Institute of Standards and Technology (NIST).[27]

Briefly, a 100 mm silicon wafer was coated with 100 μm thick layer of photoresist (SU-8 2075, Microchem, West Borough, MA, USA). Topographic patterns were created in SU8-coated wafers following laser pattern writing (Heidelberg Instruments DWL 2000) and development (in SU8 developer, Microchem). Master wafers were then derivatized with trichloro-1, 1, 2, 2, perflorocytylsilane (Sigma-Aldrich, St. Louis, MO, USA) in a vacuum chamber to facilitate release of materials cast on the patterns. Sylgard 184 elastomer (10:1 base:crosslinker) was poured over the silicon master wafer and cured overnight at 75 C. A flat piece of PDMS was also cast in a petri dish to serve as the substrate for the bottom of the microchannels. Prior to bonding, inlet ports were created using a 0.75 mm Harris Micro-Punch. PDMS layers were bonded together following treatment with oxygen plasma (Plasmatic Systems Inc, USA). The waveguide channels of the device were filled with optical adhesive (Norland Optical Adhesive 88, Norland Products, Cranbury NJ) and degassed. Stripped and cleaved optical fibers (FG105UCA, Thorlabs, Newton, NJ, USA) were inserted into the tapered ends of the waveguide channel followed by curing of optical adhesive with a UV lamp. See the companion paper Ref. 28 for more details on fabrication. See also Refs. 29 and 30 for related methods.

2. Materials and equipment used during operation

A fiber-coupled diode laser (488 nm-60 mW, Omicron-Laserage, Rodgau-Dudenhofen Germany) and photodetectors (918D-SL-OD2R, Newport Corporation, Irvine, CA, USA) coupled to a power meter (2936-R, Newport Corporation) were attached to fibers to deliver and measure light, respectively, from optofluidic devices. Fluorescein (30181, Sigma Aldrich, St. Louis, MO, USA; F36915, Thermo Fisher Scientific) was mixed in phosphate buffered saline (Thermo Fisher Scientific). Volumetric flow rates were controlled via gravity on a motorized Z-stage (LTS300, Thorlabs) or a syringe pump (Pump 11 Pico Plus Elite, Harvard Apparatus, Holliston, MA, USA) and monitored in series with a calibrated flow meter (LG16-0150D or LG16-0430D, Sensirion AG, Staefa ZH, Switzerland) or a microbalance (XE105T Mettler-Toledo GmbH, Greifensee, Switzerland). The complete system was controlled via Labview software. Although not necessary for actual measurements, an optical microscope (Zeiss Axio Zoom.V16) was used to image the fluorescence emission of fluorescein by the optical waveguides. See the companion paper Ref. 28 for more details on equipment and operation.

B. Results and Data Analysis

Using the microfluidic devices described above, we realized flow rate measurements for a solution of fluorescein, a fluorescent dye that, when stimulated by 488 nm light, emits 520 nm light. Critically, for our measurement process, fluorescein is also destroyed when the molecules receive high dosage of light (either due to high excitation power or slow velocity through the excitation beam), as illustrated in Fig. 5. Due to no-slip boundary condition of pressure driven flow in this device, a parabolic velocity profile is created across the channel. Molecules on

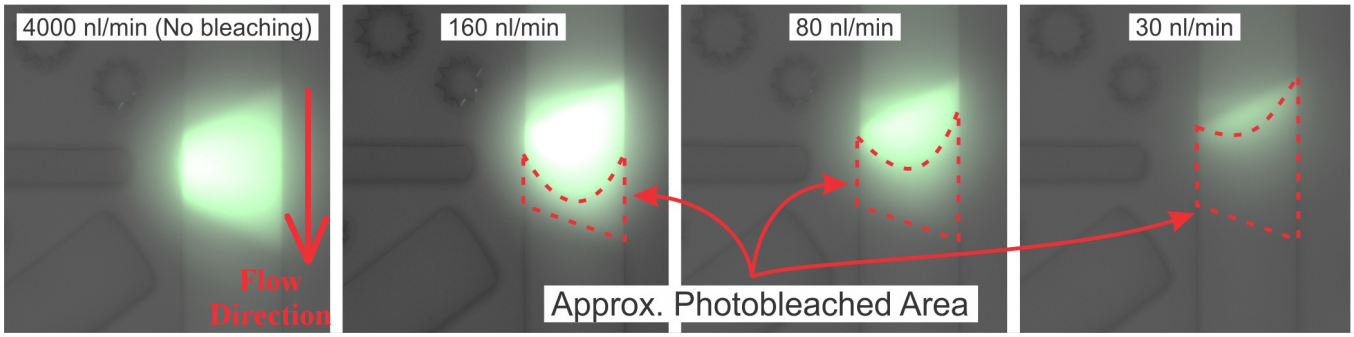

FIG. 5. Microscopy images of different flow rates exposed to 488 nm laser light (15 mW). At high flow rates, fluorescein molecules move through the laser quickly and do not photobleach, thus showing the profile of the excitation light through the channel (LEFT). As flow rate decreases, light dosage increases and photobleaching becomes evident, particularly near the channel walls where flow velocity is slowest.

edge of the channel have zero velocity and are quickly bleached, while molecules at the center of the channel move the fastest and are bleached further downstream (if at all). We explored the scaling relationship across different dosages by measuring fluorescence efficiency across a range of excitation powers and flow rates. Namely, excitation laser was stepped from 0 to 15 mW in 5% increments for each flow rates tested between roughly 5 nl/min to 1000 nl/min. A plot of fluorescence efficiency versus dosage is shown in Fig. 6. As dosage increased, either due to increased laser power or decreased flow rate, more fluorescein molecules photobleached, resulting in a decreased fluorescence efficiency.

To characterize the accuracy of measurements made on the basis of the scaling argument, we used 4 datasets (corresponding to flow rates of roughly 740 nL/min, 612 nL/min, 485 nL/min, and 358 nL/min) to generate a "master curve" by fitting the data to a convex, piecewise linear function; see Fig. 6, as well as Appendix B for details of the fitting routine. Here the use of a convex function is motivated by the linear model Eq. (16), as well as empirically observed properties of the data. Of note, we set $f(p) = p^{1.174}$ as determined by the optimization routine discussed in Appendix B, which is consistent with the values found in Ref. 17. Importantly, the dosages as determined via the Sensirion flow meter have 5% relative error or less at the calibration flow rates, which is consistent with variation of the data about the master curve. To convert this to uncertainty in flow rates, we observe that

$$v_v = \frac{f(p)}{\bar{\xi} \pm \epsilon_\xi} \approx \frac{f(p)}{\bar{\xi}} \left[1 \mp \frac{\epsilon_\xi}{\bar{\xi}}\right], \tag{30}$$

where $\bar{\xi}$ is the expected value of ξ and ϵ_ξ is a corresponding uncertainty. Notably, Eq. (30) implies that to leading order, the relative uncertainty in dosage is equal to the relative uncertainty in the volumetric flow rate. Based on the theory of Sec. V, we therefore expect a lower limit on the uncertainty of the scaling measurements to be 5%.

To test this on flow rates below the calibration rates, we used a gravimetric correction (i.e. based on the height of the source water column) to provide reference flow rates, which are accurate to 5% down to 10 nL/min and 10% at 5 nL/min.[28] Next, we used the master curve and Eq. (25) to measure flow rates using our optofluidic flowmeter and then computed the relative errors

$$\epsilon_{\text{rel}} = \frac{v_{\text{grav}} - v_{\text{opto}}}{v_{\text{grav}}}, \tag{31}$$

where v_{grav} is the gravimetric estimate and v_{opto} is the optofluidic measurement. See Fig. 7 for results of this exercise.[31] Remarkably, the optofluidic flowmeter is to accurate relative to the gravimetric measurements to within roughly 6 % down to 28 nL/min. Moreover, examination of the figure shows that the 5 nL/min efficiencies also fall onto the collapsed data, suggesting that viable measurements can be performed down to this flow rate. A more detailed analysis of such measurements and their corresponding uncertainties is reserved for a forthcoming manuscript.

VIII. DISCUSSION AND CONCLUSIONS

A. Comparison with other measurement techniques

1. *On model-form errors*

It is a general fact that all measurements, no matter how simple, require an underlying model to convert raw data into an estimate of the quantity of interest. Thus, the UQ community has come to recognize that *model-form error* – i.e. the discrepancy between a model and reality – is a fundamental part of any uncertainty budget. With this in mind, one of our main objectives is to demonstrate that our scaling approach eliminates a large portion of such uncertainties and thereby improves the robustness of flow rate measurements. We highlight this conclusion by way of comparison.

In more detail, consider a generic setting in which: (i) a model takes the system geometry and/or other param-

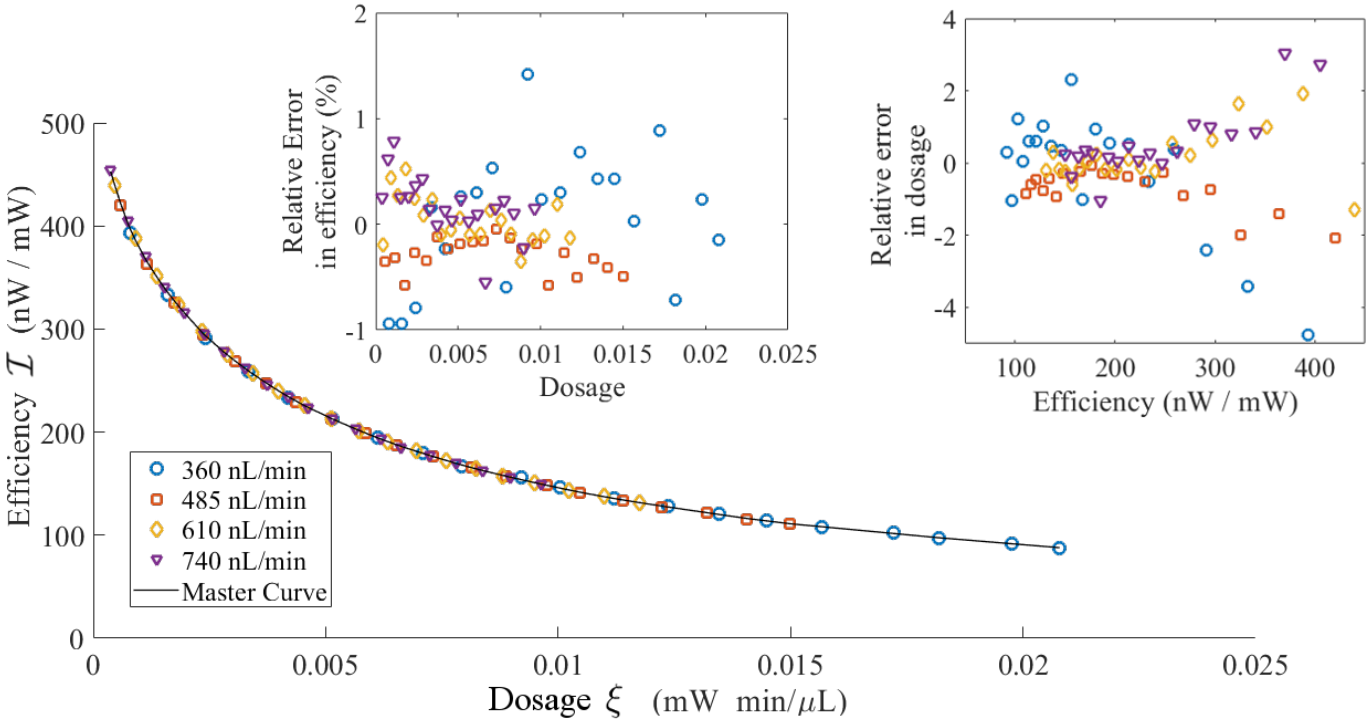

FIG. 6. Example of an experimentally obtained master calibration curve (black) for a flowmeter of the type illustrated in Fig. 1. Fluorescence efficiency (emission per excitation power) was measured in 5% increments of laser power from 0 mW to 15 mW at four flow rates (740 nL/min, 610 nL/min, 485 nL/min, 360 nL/min), which were recorded on a height-corrected Sensirion (HCS) flowmeter with 5% uncertainty. For clarity, horizontal error bars in the data points are not shown, but would span an interval of ± 5 % of the dosage of a given data point. The master curve was generated using the convex optimization routine discussed in Appendix B. The insets provide a more details on variation in the data, which is a surrogate for uncertainties associated with the measurement procedure. *Top Left:* Error in the measured efficiences relative to the master curve (i.e. "vertical residuals"). Note that the relative errors are bounded by roughly 1 %, consistent with the specifications of the Newport Power Meter. *Top Right:* Error in the measured dosages relative to the master curve (i.e. "horizontal residuals"). The error in the data relative to the curve is on the order of 5 % or less, consistent with the HCS.

eters λ as inputs and determines v_v as an output; and (ii) subsequently uses this flow rate (or the underlying model solution) to predict the outcome (i.e. raw signal) S of an idealized measurement. Typically such approaches are used as the basis for measurement in the same way as our scaling approach. That is, S has a one-to-one correspondence with v_v, *but subject to the assumption that the model exactly describes the experimental setup.* Without loss of generality, we can recast this observation by stating that $v_v = v_v(\lambda, S)$ is a function of both S and the model parameters λ, where the latter are assumed to be known exactly.

From a measurement perspective, this joint dependence is problematic insofar as v_v gains additional uncertainties arising from our inability to perfectly know λ. Moreover, we anticipate that for a fixed method of characterizing the system dimensions, their corresponding relative uncertainty increases with decreasing system sizes and can in fact be unbounded.[32] In contrast to the scaling method, uncertainties in v_v can therefore be large, if not divergent. Ultimately, we attribute this problem to a breakdown of the assumption that the model describes the experiment, i.e. that we know λ with any meaningful certainty.

A simple example illustrates this point. Assume that for a fixed system geometry, a model computes the z-component v of the fluid velocity of a steady-state Poiseuille flow by solving

$$v_{xx} + v_{yy} = -P_z \tag{32}$$

where the duct has a square cross-section, P_z is the pressure gradient in the z-direction, and all of the relevant physical constants have been set to one. For completeness, we also posit a generic boundary condition of the form $\mathcal{B}(v) = 0$, where $\mathcal{B}$ (which has nothing to do with bleaching in this context) is some function of v and its derivatives.

Now, typical measurements of the system geometry (e.g. using microscopy) return the position of the boundary to within some *absolute* uncertainty, so that we may

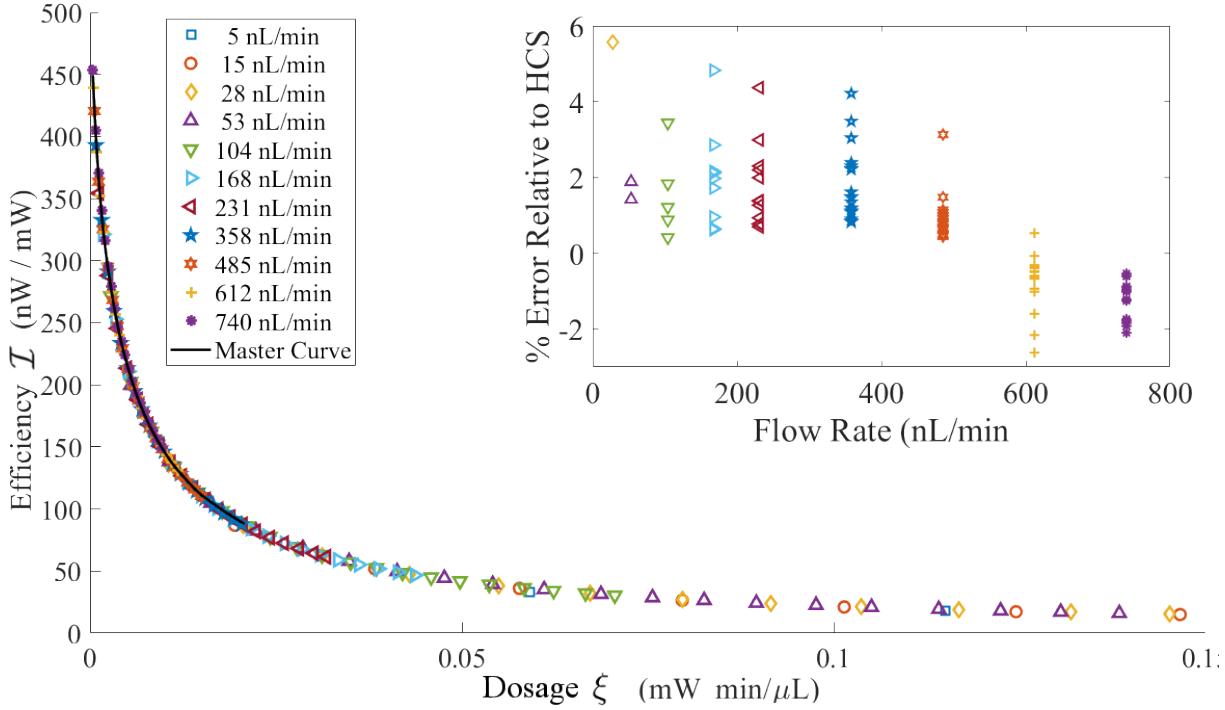

FIG. 7. Master curve shown in Fig. 7, but superimposed on a collection of datasets having flow rates down to roughtly 5 nL/min as measured by the height-corrected Sensirion (HCS). For clarity, horizontal error bars are not shown but would span 5% of the dosage value of each datapoint, with the exception of the 5 nL/min data, for which the error bars would be 10%. Note that all of the data collapses onto a single curve that is well-described by the master curve at low dosages. As a result, we can use the measurement procedure described in Sec. III (with $f(p) = p^{1.174}$) to estimate flow rates down to roughly 28 nL/min. The inset shows the errors in these measurements relative to the HCS, which remarkably agree to within 6 % for all measurements.

write

$$0 \leq x, y \leq a \pm \epsilon_a \tag{33}$$

for some constant a and its associated uncertainty ϵ_a. For our purposes, however, it is more convenient to express the upper bound in terms of the relative uncertainty

$$r_a = \epsilon_a / a \tag{34}$$

which implies $x \leq a(1 \pm r_a)$ and similarly for y. Rescaling Eq. (32) in terms of the boundary values by defining

$$x = (1 \pm r_a)\hat{x} \tag{35a}$$
$$y = (1 \pm r_a)\hat{y} \tag{35b}$$

now yields

$$(\hat{v}_{\hat{x}\hat{x}} + \hat{v}_{\hat{y}\hat{y}}) = -p_z \tag{36a}$$
$$0 \leq x, y \leq a, \tag{36b}$$

where $\hat{v} = v/(1 \pm r_a)^2$ is the "true" value of the flow rate.

To understand better how the error r_a has propagated into v, note that setting $r_a = 0$ (for fixed a) corresponds to an absolute error of zero, i.e. an ideal, accurate solution. Therefore, taking the ratio $v/\hat{v} - 1 = \pm r_a + r_a^2$ shows that the relative error in the velocity goes as r_a^2 for large relative uncertainty. *However, this uncertainty grows as we shrink the system dimensions, so that the model's ability to match the experimental setup diminishes with size. Thus, model-form error eventually dominates the measurement.*

In contrast to this, the scaling approach we advocate remains faithful to the underlying experiment, even as the system-size decreases. Ultimately this arises from the fact that the method does not actually need to know the system size except to within perhaps a factor of two, or in more illuminating terms, to within 100 % relative error. More generally, the scaling approach makes fewer and more general assumptions than many other techniques. That being said, our approach still suffers from its own unique sources of uncertainty, e.g. arising from fluorescence intensity measurements. Arguably these signals will decrease in magnitude as system sizes become smaller, but alternatives exist for addressing this problem, e.g. increasing the fluorescein concentration. Nonetheless, a more in-depth comparative study is needed to assess the relative accuracy of the scaling approach; we leave such work for an upcoming manuscript.

2. Practical issues of fabrication and operation

It is noteworthy that Eq. (19) only assumes: (i) a fixed system geometry, laser profile, and fluorescence detector; (ii) a Pouiseille flow at reasonable Reynolds number; and (iii) information about the bleaching rate dependence on power, i.e. $f(p)$. From a practical standpoint these assumptions impose few requirements on the fabrication process, which facilitates scalability of the measurement procedure. Indeed, our initial measurement devices were cast from PDMS using a process that could easily be scaled in an industrial setting.

In contrast, methods that invoke detailed models to measure flow rates (e.g. in the spirit of the previous section) invariably require accurate characterization of the device geometry. Notably, non-destructive and fully three-dimensional characterization (e.g. using tomography) may be too expensive for individual commercial products. It is more likely that such techniques would rely on "make-it and break-it" characterization of several representative devices to inform statistical models of the device geometry, which contribute to the uncertainty budget as described above. Moreover, non-trivial geometries would likely require numerical PDE solvers to predict raw measurement signals corresponding to v_v. Importantly, the scaling approach avoids these fabrication and operation issues altogether.

Questions of economics aside, the scaling method is also attractive because it offers the possibility of small-scale, continuous, and in-situ measurement capabilities, which are currently an elusive goal in the microfluidics community. As illustrated in Sec. VII, waveguides needed to carry the laser-light and fluorescence signals are on the same length-scale as the microchannel and can be inserted into the device in a non-obtrusive manner. Thus, it is straightforward to incorporate multiple flow-meters into any given channel at different points along the flow-path, or even measure flow rates in separate forks of a channel. The corresponding fluorescence signals are likewise straightforward to measure using commercial (and relatively inexpensive) power meters. Notably, this level of simplicity should facilitate automation of measurements.

B. Bootstrapping device calibration

Back-of-the-envelope calculations and experimental results indicate that any given device may have a domain of validity encompassing at least two orders of magnitude in flow rates. The exception to this is the postulated Taylor-Aris device, which does not have a theoretical lower-bound on flow rate, although practical considerations will likely enforce one.

With this in mind, we recognize that the domain-of-validity of a given device can be extended through a "serial-bootstrap" fabrication. In particular, we can imagine N flow-meters in series with one another along a channel that discretely decreases in width between each meter. This can be done in such a way that the domains of validity of any adjacent meters partially overlap, but with each downstream meter able to measure lower flow rates. The overlap in measurement capabilities means that the first meter can be used to calibrate the second, which can be used to calibrate the third, and so on. A benefit of this approach is that we can obtain two separate (but not completely independent) measurements of a flow rate when it falls into the domains-of-validity of two adjacent meters. Given that microfluidic channels can foul and otherwise be degraded, this redundancy allows a certain degree of diagnostic capability to assess the status of a given measurement device.

C. Limitations and open problems

As suggested throughout, a key limitation of the scaling approach is the requirement that the system be in a advection-dominated or Taylor-Aris regime. While we have demonstrated that such devices can in fact be constructed, there are several additional assumptions that may be problematic.

In particular, the analysis assumes that the system geometry is independent of the flow rate. For small changes around v_r, this assumption is likely valid. However, channels made from flexible, polymeric materials may deform under higher pressures needed to reach fast flow rates. Thus, consideration should be given to the operating regimes and elastic modulus of the materials to ensure that such issues do not affect measurements.

A somewhat prominent assumption of our model is the requirement that $I_{k,s}$ be scaled by p in order to determine the measurement signal $\mathcal{I}$. Physically, we expect the linear approximation to be valid for dilute solutions of fluorescein, since the majority of the light is likely to pass through the fluid. In other words, we *anticipate* that only an infinitesimal number of photons are absorbed, so that an increase in p should yield a proportional increase in fluorescence. Mathematically this assumption can be relaxed by postulating that

$$I_s = \int \mathrm{d}\mathbf{r}\, h(p) F(c, \mathbf{r}), \tag{37}$$

where $h(p)$ is some monotone function in the laser power, which leads to a modified definition $\mathcal{I} = I_s/h(p)$. Thus, the choice of $h(p)$ becomes a modeling assumption that must be validated against experimental data. To the best of our understanding, model-form error associated with this choice cannot be eliminated without more information about the physics of photobleaching and fluorescence.

Lastly, we recognize that some microfluidic settings require measurements of v_v in systems with unsteady and/or variable flow rates. While the steady-state assumption would seem to exclude our approach in such

cases, further specification of what we mean by "variable" is necessary. In particular, upon changing the flow rate there is some characteristic time over which the fluorescence signal reverts to its steady-state value. Provided the rate of change of the flow rate is slow relative to this characteristic time, our method is likely applicable. However, further exploration of this topic is beyond the scope of this work and is reserved for a future manuscript.

Acknowledgements: The authors wish to thank Drs. Ryan Evans, John Wright, Charles Romine, and Geoffrey McFadden for useful discussions during the preparation of this manuscript. We also thank Steve Meek and James Hands for help with device fabrication. This work is a contribution of the National Institute of Standards and Technology, and as such, is not subject to copyright in the United States of America.

Appendix A: Monotonicity Lemma

Consider the differential equation

$$\frac{\mathrm{d}c}{\mathrm{d}z} = -g(\xi)B(c,z), \tag{A1}$$

where

- $\xi > 0$;
- $0 < B(c,z) < M$ for $c > 0$ and $0 \leq z \leq z_{\max}$ for some maximum value of z and $M < \infty$;
- $B(0,z) = 0$;
- $g(\xi) > 0$ is strongly monotone in ξ.
- $B(c,z)$ is continuous and differentiable in c and z;
- and $c(0) = c_0$ for some constant $c_0 > 0$ and all ξ.

We show that for fixed $z > 0$, c is strictly monotone decreasing in ξ.

Proof by contradiction: The hypotheses above imply that there exists a unique solution c to Eq. (A1); moreover, this c is continuous and has a continuous derivative.[21] With this in mind, it is obvious that c is a monotone decreasing function of z. Moreover, it is clear that for a fixed z, c can be parameterized in terms of ξ. Finally, note that $c > 0$ for all $z > 0$, since B is positive and bounded, but also vanishes as $c \to 0$.

Now, let c_1 be the solution corresponding to ξ_1 and c_2 the solution corresponding to ξ_2. Let $\xi_1 > \xi_2$ and recall that $c_1(z) = c_2(z) = c_0$ for $z = 0$. Note therefore that the difference

$$\left.\frac{d(c_1 - c_2)}{dz}\right|_{z=0} = [g(\xi_2) - g(\xi_1)]B(c_0, 0) < 0 \tag{A2}$$

by monotonicity of g. Moreover, $c_1 - c_2$ is continuous and has a continuous derivative. Thus, there exists a δ such that

$$\frac{d(c_1 - c_2)}{dz} < 0 \tag{A3}$$

for all $z \in [0, \delta]$. Integrating, we find that $c_1 - c_2 < 0$ for all $z \in (0, \delta]$. Thus, there exists some finite domain over which $c_1 < c_2$.

Now, two possibilities exist. Either $c_1 < c_2$ for all $z > 0$ or there is some first point $z_0 > \delta$ such that $c_1(z_0) = c_2(z_0)$. In the former case, we have the required condition that c is monotone decreasing in ξ for fixed z. So we only consider the second case.

If z_0 is the first point for which $c_1 = c_2$ (aside from $z = 0$), then we have again that

$$\left.\frac{d(c_1 - c_2)}{dz}\right|_{z=z_0} < 0 \tag{A4}$$

since $B(c_1, z_0) = B(c_2, z_0)$. Again by continuity of c and its derivative, there exists some δ_0 such that $\frac{d(c_1 - c_2)}{dz} < 0$ for all $x \in [z_0 - \delta_0, z_0]$. Since $c_1(z_0 - \delta_0) - c_2(z_0 - \delta_0) < 0$ by assumption, integrating from $z_0 - \delta_0$ to z_0 yields the conclusion that $c_1(z_0) - c_2(z_0) < 0$, which is a contradiction. Thus, c_1 does not intersect c_2 at any $z > 0$.

Appendix B: Convex Reconstructions of the Master Curve

Without any detailed knowledge of the system geometry or laser profile, it is impossible to predict the exact functional form of the fluorescence efficiency. However, Eq. (16) and Fig. 6 have the general property of being convex, which, loosely speaking, means that the second derivative of $\mathcal{I}(\xi)$ is non-negative. With this in mind, we can generate an analytical representation of master curve in terms of the solution to a convex optimization problem.

Specifically, let $(\xi_i, \mathcal{I}_i)$ denote an ordered pair of dosage and efficiency values associated with the ith experiment, and assume that we have N such pairs (i.e. $1 \leq i \leq N$). We posit that the $\mathcal{I}_i$ have some errors relative to a true value $\hat{\mathcal{I}}_i$, which we wish to estimate. Importantly, we postulate that these $\hat{\mathcal{I}}_i$ all lie on a convex function $\hat{\mathcal{I}}(\xi)$ that interpolates the available data.

Now, in general there is no unique convex function that fits a set of data by minimizing an objective function such as the sum-of-squared-differences.[33] However, the piecewise linear function that interpolates the $\hat{\mathcal{I}}_i$ is an upper bound on all such convex functions. Moreover, in the case of a dense grid of dosages ξ_i, the variation between all such curves is negligible. From a practical standpoint, it is therefore sufficient to solve the quadratic

programming problem that minimizes the objective

$$\mathcal{L} = \frac{1}{2}\hat{\boldsymbol{\mathcal{I}}}^{\mathrm{T}}\mathbb{I}\hat{\boldsymbol{\mathcal{I}}} - 2\hat{\boldsymbol{\mathcal{I}}}^{\mathrm{T}}\boldsymbol{\mathcal{I}} \tag{B1a}$$

$$\mathbf{A}\hat{\boldsymbol{\mathcal{I}}} \geq 0 \tag{B1b}$$

as a function of $\hat{\boldsymbol{\mathcal{I}}}$, where $\mathbb{I}$ is the $N \times N$ identity matrix, $\boldsymbol{\mathcal{I}}^{\mathrm{T}} = (\mathcal{I}_1, \mathcal{I}_2, ..., \mathcal{I}_N)$, etc. Here A is a matrix having rows that correspond to second-order finite differences. Of note, when the dosages ξ_i are not uniformly spaced (as is the case with our data), the jth row of $\mathbf{A}$ has elements that solve the linear system

$$A_{j,j-1} + A_{j,j} + A_{j,j+1} = 0 \tag{B2a}$$

$$A_{j,j-1}(\xi_{j-1} - \xi_j) + A_{j,j+1}(\xi_{j+1} - \xi_j) = 0 \tag{B2b}$$

$$A_{j,j-1}(\xi_{j-1} - \xi_j)^2 + A_{j,j+1}(\xi_{j+1} - \xi_j)^2 = 1, \tag{B2c}$$

which is valid for $1 < j < N$ and comes from the requirement that $\mathbf{A}\boldsymbol{\mathcal{I}}$ be a "central" second-order finite difference of $\boldsymbol{\mathcal{I}}$ on the nonuniform grid of ξ. For $j = 1$ and $j = N$, analogous linear systems can be derived for non-central finite differences to determine the corresponding matrix elements. This task is left as an exercise for the reader.

To determine the functional form of $f(p)$, we reformulate the optimization by allowing $\xi_i = f(p_i)/v_i$ for some function f parameterized in terms of unknown coefficients (v_i are the corresponding flow rates). In our case, we set $f(p) = p^q$ for an unknown power q and minimize the objective $\mathcal{L}(\hat{\boldsymbol{\mathcal{I}}}, q)$ as a function of the efficiencies and q.

[1] Yung-Chieh Tan, Jeffrey S. Fisher, Alan I. Lee, Vittorio Cristini, and Abraham Phillip Lee, "Design of microfluidic channel geometries for the control of droplet volume, chemical concentration, and sorting," Lab Chip **4**, 292–298 (2004).

[2] Guofeng Guan, Lidan Wu, Ali Asgar Bhagat, Zirui Li, Peter C. Y. Chen, Shuzhe Chao, Chong Jin Ong, and Jongyoon Han, "Spiral microchannel with rectangular and trapezoidal cross-sections for size based particle separation," Scientific Reports **3**, 1475 EP – (2013).

[3] Brian K. McKenna, James G. Evans, Man Ching Cheung, and Daniel J. Ehrlich, "A parallel microfluidic flow cytometer for high-content screening," Nature Methods **8**, 401 EP – (2011).

[4] Volker Hessel, Holger Lwe, and Friedhelm Schnfeld, "Micromixersa review on passive and active mixing principles," Chemical Engineering Science **60**, 2479 – 2501 (2005), 5th International Symposium on Mixing in Industrial Processes (ISMIP5).

[5] Mohammad Sadegh Cheri, Hamid Latifi, Jalal Sadeghi, Mohammadreza Salehi Moghaddam, Hamidreza Shahraki, and Hasan Hajghassem, "Real-time measurement of flow rate in microfluidic devices using a cantilever-based optofluidic sensor," Analyst **139**, 431–438 (2014).

[6] Haoli Wang and Yuan Wang, "Measurement of water flow rate in microchannels based on the microfluidic particle image velocimetry," Measurement **42**, 119 – 126 (2009).

[7] More precisely, we prove existence of a *measurement signal* whose salient feature does not depend on the detailed information about the system (aside from v_v). Whether a measurement of the signal can actually be performed is an experimental issue.

[8] This is often called model-form error in the UQ community.

[9] Technically speaking, ξ is the dosage per-unit-volume.

[10] E. Gaughan, *Introduction to Analysis*, Pure and applied undergraduate texts (American Mathematical Society, 1998).

[11] C.M. Bender and S.A. Orszag, *Advanced Mathematical Methods for Scientists and Engineers I: Asymptotic Methods and Perturbation Theory*, Advanced Mathematical Methods for Scientists and Engineers (Springer, 1978).

[12] M Ahrens, St Klein, B Nestler, and C Damiani, "Design and uncertainty assessment of a setup for calibration of microfluidic devices down to 5nlmin 1," Measurement Science and Technology **25**, 015301 (2014).

[13] While not really essential, we assume that the kth intensity meter only collects fluorescent light emitted by molecules in the path of the *kth* laser beam.

[14] S. Gavrilyuk, S. Polyutov, P. C. Jha, Z. Rinkevicius, H. gren, and F. Gel'mukhanov, "Many-photon dynamics of photobleaching," The Journal of Physical Chemistry A **111**, 11961–11975 (2007).

[15] S. Kalies, K. Kuetemeyer, and A. Heisterkamp, "Mechanisms of high-order photobleaching and its relationship to intracellular ablation," Biomed. Opt. Express **2**, 805–816 (2011).

[16] P.S. Dittrich and P. Schwille, "Photobleaching and stabilization of. fluorophores used for single-molecule analysis. with one- and two-photon excitation," Applied Physics B **73**, 829–837 (2001).

[17] George H. Patterson and David W. Piston, "Photobleaching in two-photon excitation microscopy," Biophysical Journal **78**, 2159 – 2162 (2000).

[18] Xavier Michalet, Achillefs N. Kapanidis, Ted Laurence, Fabien Pinaud, Soeren Doose, Malte Pflughoefft, and Shimon Weiss, "The power and prospects of fluorescence microscopies and spectroscopies," Annual Review of Biophysics and Biomolecular Structure **32**, 161–182 (2003).

[19] We speculate that boundedness is not necessary, but it facilitates the analysis that follows. Physically, it is not a problematic constraint because we can always assume an immeasurably large value for the bound on B.

[20] L. Song, E. J. Hennink, I. T. Young, and H. J. Tanke, "Photobleaching kinetics of fluorescein in quantitative fluorescence microscopy." Biophys J **68**, 2588–2600 (1995).

[21] M. Tenenbaum and H. Pollard, *Ordinary Differential Equations: An Elementary Textbook for Students of Mathematics, Engineering, and the Sciences*, Dover

Books on Mathematics (Dover Publications, 1963).
[22] Torvard C. Laurent, Lars-Olof Sundelof, K. Ove Wik, and Birgitta Warmegard, "Diffusion of dextran in concentrated solutions," European Journal of Biochemistry **68**, 95–102 (1976).
[23] Ruth Furukawa, Jose Luis Arauz-Lara, and Bennie R. Ware, "Self-diffusion and probe diffusion in dilute and semidilute aqueous solutions of dextran," Macromolecules **24**, 599–605 (1991).
[24] M. Arrio-Dupont, S. Cribier, G. Foucault, P. F. Devaux, and A. d'Albis, "Diffusion of fluorescently labeled macromolecules in cultured muscle cells." Biophys J **70**, 2327–2332 (1996).
[25] Gregory A. Cooksey, Christopher G. Sip, and Albert Folch, "A multi-purpose microfluidic perfusion system with combinatorial choice of inputs, mixtures, gradient patterns, and flow rates," Lab Chip **9**, 417–426 (2009).
[26] J. Cooper McDonald, David C. Duffy, Janelle R. Anderson, Daniel T. Chiu, Hongkai Wu, Olivier J. A. Schueller, and George M. Whitesides, "Fabrication of microfluidic systems in poly(dimethylsiloxane)," Electrophoresis **21**, 27–40.
[27] Certain commercial equipment, instruments, or materials are identified in this paper in order to specify the experimental procedure adequately. Such identification is not intended to imply recommendation or endorsement by the National Institute of Standards and Technology, nor is it intended to imply that the materials or equipment identified are necessarily the best available for the purpose.
[28] Gregory A. Cooksey, Paul N. Patrone, and A. Kearsley, "Dynamic measurement of nanoflows: Realization of a multidecadal optofluidic flow meter to 1 nl/min," In Preparation.
[29] S. Camou, H. Fujita, and T. Fujii, "PDMS 2d optical lens integrated with microfluidic channels: principle and characterization," Lab Chip **3**, 40–45 (2003).
[30] Thitaphat Ngernsutivorakul, Cynthia M. Cipolla, Colleen E. Dugan, Shi Jin, Michael D. Morris, Robert T. Kennedy, and Francis W. L. Esmonde-White, "Design and microfabrication of a miniature fiber optic probe with integrated lenses and mirrors for raman and fluorescence measurements," Analytical and Bioanalytical Chemistry **409**, 275–285 (2017).
[31] With the exception of the 28 nL/min datapoint (for which we can only perform one measurement), we discard the dosages associated with 5% power because the laser tends to be unstable at that setting.
[32] This is essentially an observation about the resolution limitations of imaging processes. There will always be a smallest practical lengthscale – for example, a pixel size – below which the position of an object cannot be resolved. Thus, relative uncertainty in the separation between objects grows as they approach one another.
[33] Paul Patrone, Anthony Kearsley, and Andrew Dienstfrey (American Institute of Aeronautics and Astronautics, 2018) Chap. The role of data analysis in uncertainty quantification: case studies for materials modeling.